# Project 3-4: Ultra Relativistic Fluids in 1D and 2D

Graham Reid

August 8, 2013

## 1 Introduction

These projects investigate the evolution of a relativistic fluid with an ultra relativistic equation of state. Due to the similarities between the 1D and 2D cases, the write up for both are presented here.

## 2 Equations of Motion

The equations of motion are derived from the conservation of energy and momentum and the conservation of particles [1, 2]:

$$\nabla_b T^{ab} = 0 \tag{1}$$
$$\nabla_a (\rho^a) = 0 \tag{2}$$

For a perfect fluid, the stress energy tensor can be written as:

$$T^{ab} = (\rho + P)\, u^a u^b + P g^{ab} \tag{3}$$

In these projects we restrict our attention to Minkowski space so that the metric is given by its usual cartesian form. In addition to the conservation equations above, we must have an equation of state to relate the pressure to our other fluid variables. For simplicity, we consider an ultra relativistic fluid (we assume that the internal energy density of the fluid is much larger than the rest mass density $\rho_0 \epsilon \gg \rho_0$):

$$P = (\Gamma - 1)\rho \tag{4}$$

In the above equation, $\Gamma$ is the adiabatic index which will be taken to be a constant in the range $(1, 2]$. When the fluid is ultra relativistic, the number of particles no longer needs to be conserved and the only equation we need to consider is the conservation of energy-momentum [1]. Introducing the conservative

variables:

$$\begin{aligned} \tau &= (\rho + P)W^2 - P && (5)\\ S_x &= v_x(\tau + P) && (6)\\ S_y &= v_y(\tau + P) && (7)\\ W &= (1 - v^2)^{-1/2} && (8) \end{aligned}$$

The relevant stress energy components become:

$$\begin{aligned} T^{00} &= \tau && (9)\\ T^{01} &= T^{10} = S_x && (10)\\ T^{02} &= T^{20} = S_y && (11)\\ T^{11} &= S_x v_x + P && (12)\\ T^{22} &= Sy_v y + P && (13)\\ T^{12} &= T^{21} = S_x v_y = S_y v_x && (14) \end{aligned}$$

The non-trivial equations of motion are:

$$\begin{aligned} \partial_t \tau + \partial_x(v_x(\tau + P)) + \partial_y(v_y(\tau + P)) = 0 && (15)\\ \partial_t Sx + \partial_x(S_x v_x + P) + \partial_y(S_x v_y) = 0 && (16)\\ \partial_t Sy + \partial_x(S_y v_x) + \partial_y(S_y v_y + P) = 0 && (17) \end{aligned}$$

The equations shown above are prone to shocks even when the initial data is smooth, so simple discretizations based will not be accurate or stable. Instead of using a finite difference discretization we take a finite volume approach, treating our grid points as cells which contain a finite amount of the fluid. We then cast the equations in a form which explicitly conserves the conservative variables to within numerical accuracy. For the details of the remaining derivation please see the original handouts [1] and [2]. For a great introduction of fluid solvers (and in particular the Roe solver see [3]).

It is worth noting that there is a small typo in [2]. The eigenvector denoted $l_0^y$ should have the following form:

$$l_0^y = \left[ -\frac{v_x(1 + v^2 - 2v_y^2)}{(1 - v_y^2)(1 - v^2)}, \frac{1 - v^2 + 2v_x^2}{1 - v^2}, \frac{v_x v_y(1 + v^2 - 2v_y^2)}{(1 - v_y^2)(1 - v^2)} \right] \quad (18)$$

rather than how it appears in the original document:

$$l_0^y = \left[ -\frac{v_x(1 + v^2 - 2v_y^2)}{(1 - v_y^2)(1 - v^2)}, \frac{1 - v^2 - 2v_x^2}{1 - v^2}, \frac{v_x v_y(1 + v^2 - 2v_y^2)}{(1 - v_y^2)(1 - v^2)} \right] \quad (19)$$

The differences caused by the substitution are quite subtle for low velocities and only become significant for non-slab-symmetric data at high velocities.

# 3 Numerics

For both the 1D and 2D cases a Roes solver was implemented to solve the equations of motion. This particular solver has the benefits of being second order accurate in regions of smooth data while it uses first order methods to capture shocks and prevent dissipation. The boundary conditions for the 1D and 2D models were chosen to be approximate outflow boundary conditions implemented using ghost cells. The time stepping was performed with an RK2 integrator to insure second order accuracy in $\Delta t$.

# 4 Results

## 4.1 1D fluid

Using a variety of mesh densities it was verified that the solutions obtained from the simulations were second order accurate except in the presence of local extrema and shocks. Figure 1 shows the convergence of gaussian initial data for a series of mesh refinements.

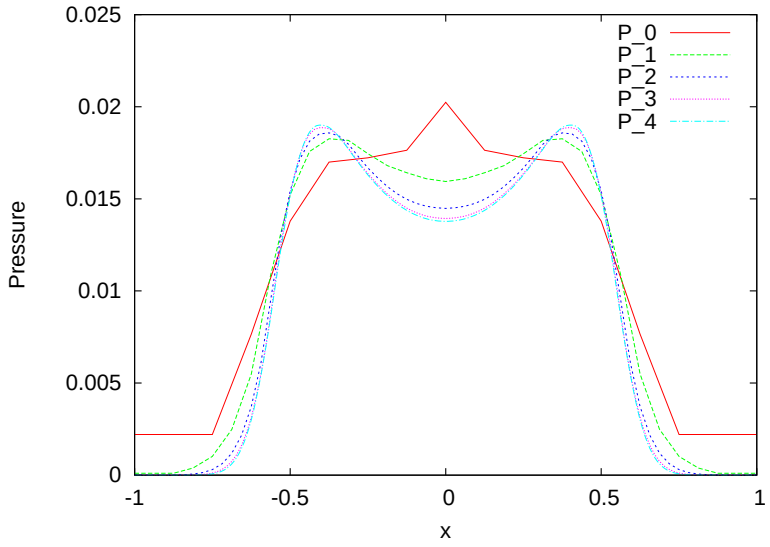


Figure 1: Convergence of the fluid solver for gaussian initial data for a series of mesh refinements.

Figure 2 demonstrates the convergence of a shock tube test to the exact solution. Although the shock front narrows as the mesh density is increased, it remains spread over approximately 10 grid points. Using a different flux limiter (such as superbee rather than minmod) may give better shock resolution.

By varying the magnitude of the density on the left hand side of the shock tube, it was determined that the maximum Lorentz Factor that could be ob-

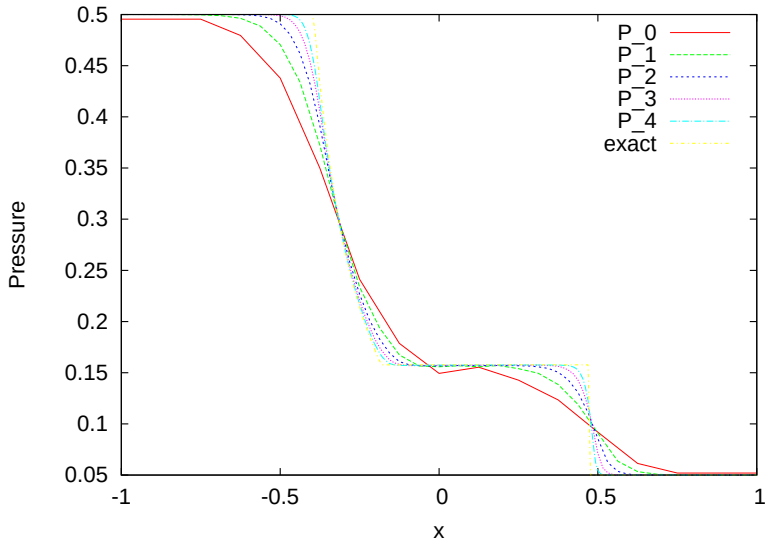


Figure 2: Convergence of the fluid solver for stock tube test for a series of mesh refinements. In the vicinity of the shock the convergence is first order.

tained was approximately $\beta = 0.98c$ corresponding to a baseline density of 0.1 with a jump of 450 across the discontinuity. At slightly higher densities gaps, the density of the fluid in the vacinity of the discontinuity goes quickly to zero driving the square of the velocity to within roundoff error of $c$. Due to the dependance of the conservative variables on $\left(1 - v^2\right)^{-1}$, a divide by zero error occurs and the relevant arrays are quickly populated by $NaN$. This maximum Lorentz Factor is robust against increases in mesh density. The obvious choices of imposing a minimum background density or additional flux limitations on cells with low densities lead to instabilities which I was unable to resolve.

## 4.2 2D fluid

After extending the 1D code, a variety of convergence tests were run on smooth initial data. As in the 1D case, the simulation was second order accurate far from local extrema and shocks and first order accurate in those regions. The results of a shock tube test are shown below in Figure 3.

An interesting pattern emerged when two jets were placed on opposite sides of the simulation region and offset from each other slightly. Figures 1 and 2 demonstrate the periodic nature of the solution obtained. Videos of this simulation as well as a demonstration of the Kelvin Helmholtz instability may be found on my website [4].

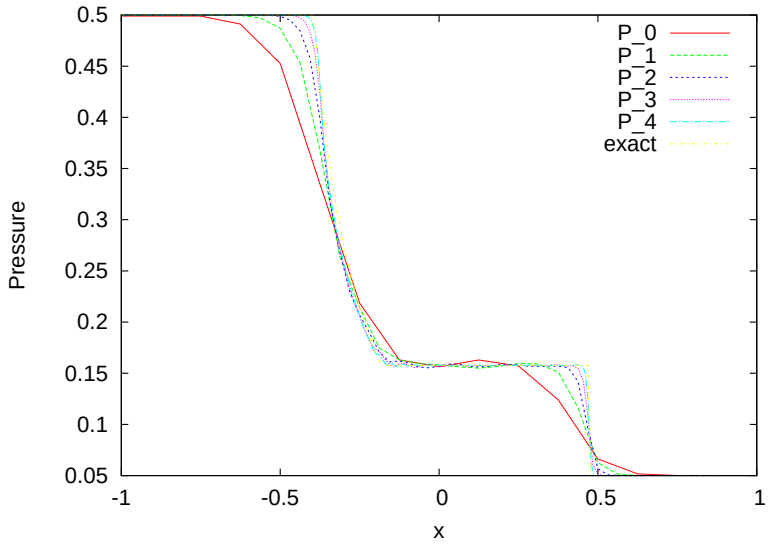


Figure 3: Convergence of the fluid solver for stock tube test for a series of mesh refinements. Here a 1D cross section is displayed. Both the 1D and 2D results converge to the exact solutions as the mesh density is increased.

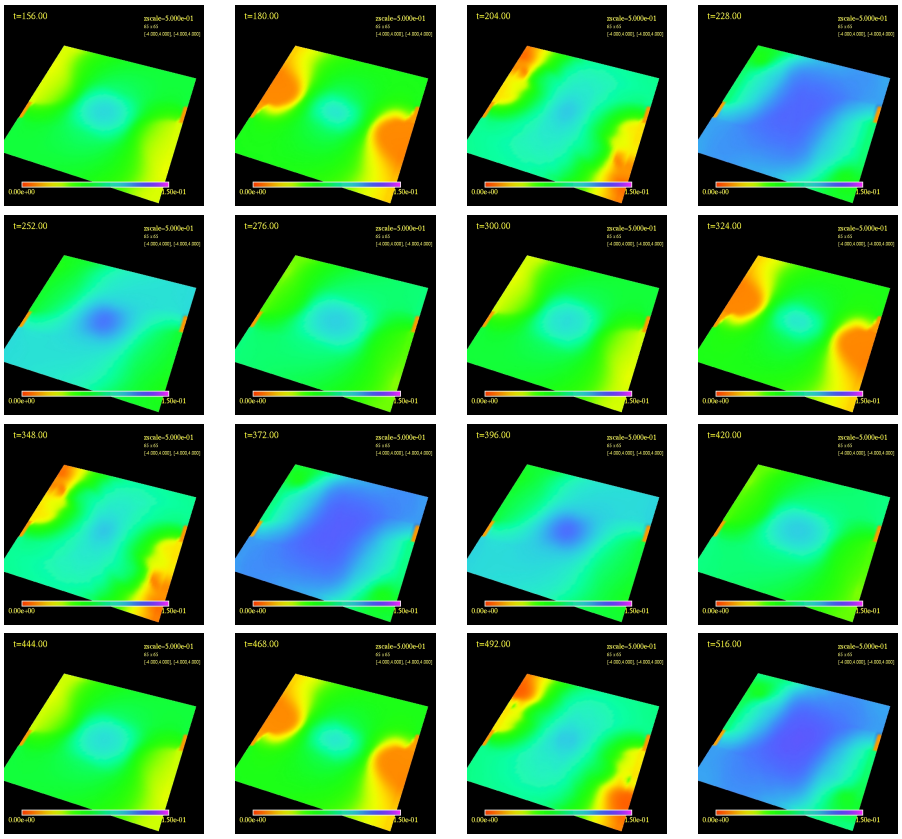


Table 1: Pressure of a Periodic solution obtained by offsetting two opposing jets from one another. The solution is characterized by the development of a high pressure center and low pressure edges which build in size and sparcity before exiting the region at highly relativistic speeds.

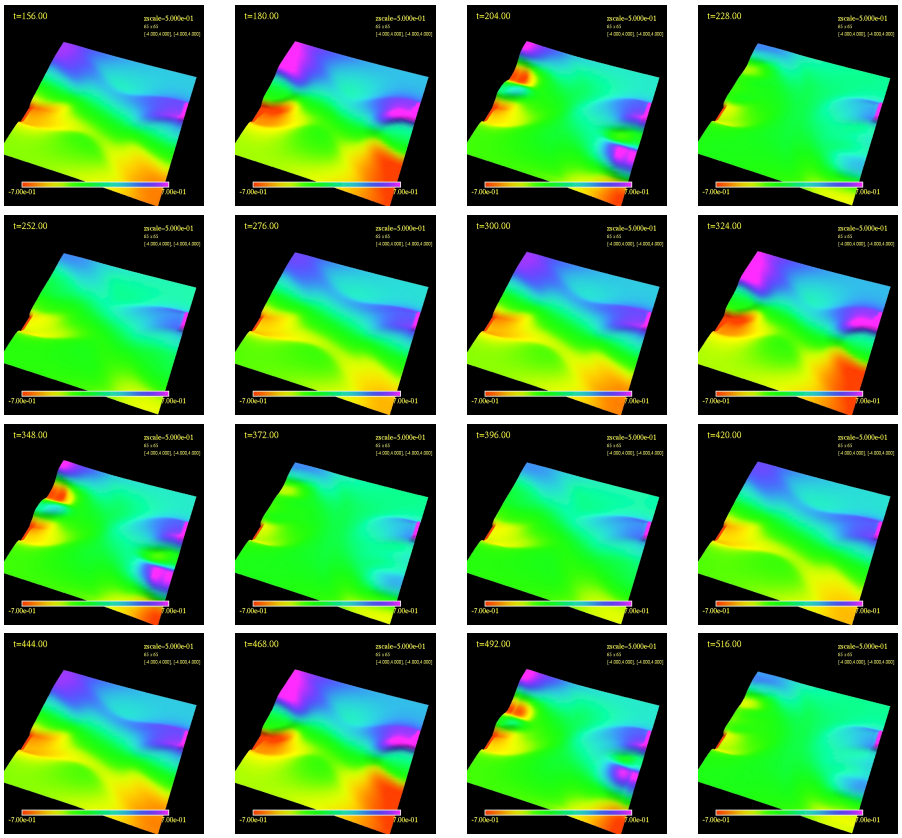


Table 2: Y velocity of the above solution.

# References


[1] M. Choptuik, "Project 2: 1d ultrarelativistic fluid," http://bh0.phas.ubc.ca/People/matt/Teaching/03Vancouver/p2.ps, 2003.

[2] ——, "Project 3(b): 2d ultrarelativistic fluid," http://bh0.phas.ubc.ca/People/matt/Teaching/03Vancouver/p3.ps, 2003.

[3] C. Dullemond, "Lecture on: Numerical fluid dynamics:," http://www.mpia.de/homes/dullemon/lectures/fluiddynamics08/, 2008.

[4] G. Reid. (2013) Projects. [Online]. Available: http://laplace.physics.ubc.ca/People/gdreid/projects.html